Light Amplification in the Single-Exciton Regime Using Exciton−Exciton Repulsion in Type-II Nanocrystal Quantum Dots

Jagjit Nanda, Sergei A. Ivanov, Marc Achermann, Ilya Bezel, Andrei Piryatinski, and Victor I. Klimov*

Los Alamos National Laboratory, Los Alamos, New Mexico 87545

Received: May 18, 2007; In Final Form: August 10, 2007

Optical gain in ultrasmall semiconductor nanocrystals requires that some of the nanoparticles in the ensemble be excited with multiple electron−hole pairs (multiexcitons). A significant complication arising from this multiexciton nature of optical amplification is the ultrafast gain decay induced by nonradiative Auger recombination. Here, we develop a simple model for analyzing optical gain in the nanocrystals in the presence of exciton−exciton (X−X) interactions. This analysis indicates that if the X−X interaction is repulsive and its energy is large compared to the ensemble line width of the emitting transition, optical gain can occur in the single-exciton regime without involvement of multiexcitons. We further analyze theoretically and experimentally X−X interactions in type-II heteronanocrystals of CdS (core)/ZnSe (shell) and ZnTe (core)/CdSe (shell) and show that they can produce giant repulsion energies of more than 100 meV resulting from a significant local charge density generated as a result of spatial separation between electrons and holes. We observe that the dynamical and spectral properties of optical gain in type-II nanocrystals are distinctly different from those of multiexciton gain in traditional type-I nanocrystals and are consistent with those expected for the single-exciton regime. An important implication of these results is the possibility of a significant increase in the optical-gain lifetime, which could simplify applications of chemically synthesized nanocrystals in practical lasing technologies and perhaps allow for lasing using electrical injection.

Introduction

Chemically synthesized semiconductor nanocrystals (NCs) known also as nanocrystal quantum dots are attractive materials for light-emitting applications including bioimaging,[1,2] light-emitting diodes,[3−5] and lasers.[6,7] NCs are nanoscale crystalline particles surrounded by a layer of organic ligand molecules. They can be considered as "quantum boxes", whose electronic and optical properties can be controlled by changing NC sizes and/or shapes.[8,9] Because of the presence of a capping layer, NCs can be manipulated chemically like large molecules. Specifically, with simple solution-based methods, NCs can be easily prepared as close-packed films (NC solids)[10] or encapsulated with high densities into polymers[11] or sol−gel glasses,[12,13] which facilitates their use in traditional fiber technologies. Further, by combining NCs with optical resonators, one can design microlasers of various configurations.[7,14−16]

Numerous observations of correlations between the NC emission efficiency and the quality of surface passivation suggest that nonradiative carrier losses in these structures are primarily due to recombination at surface defects. By using improved methods for surface treatment involving overcoating with either inorganic (core/shell NCs)[17−19] or organic[20] layers, it is possible to almost completely eliminate surface-related recombination channels, which results in NCs with near-unity emission quantum yields. Despite these favorable light-emitting properties, NCs are difficult to use in lasing applications. Because of the degeneracy of the lowest energy "emitting" levels, the population inversion in NCs can only be achieved if the average number of electron−hole pairs (excitons) per NC, $\langle N \rangle$, is greater than 1. This consideration implies that optical gain in NC media originates from nanoparticles that contain at least two electron−hole pairs (i.e., biexcitons and other multiexcitons of higher order).[6] Indeed, experimental studies of CdSe NCs indicate that optical gain in these structures is dominated by biexcitons.[21] Even higher order multiexcitons are required to produce optical gain in PbSe NCs[22] that are characterized by high, 8-fold degeneracy of the lowest electron and hole states.[23]

A serious complication arising from the multiexcitonic nature of optical gain is the high-efficiency nonradiative Auger recombination induced by carrier−carrier interactions.[6,24] In this process, the electron−hole (e−h) recombination energy is not emitted as a photon but is transferred instead to a third particle (an electron or a hole) that is re-excited to a higher energy state.[25,26] In NCs, Auger recombination is characterized by very short time constants (from a few picoseconds to a few hundreds of picoseconds)[24] that severely limit optical-gain lifetimes and preclude the use of steady-state optical or electrical pumping for obtaining NC lasing.

Potential approaches to reducing Auger rates include the use of elongated NCs (quantum rods)[27,28] or core−shell hetero-NC,[29] which enables a decreased exciton−exciton (X−X) coupling without losing the benefits of strong quantum confinement. However, the most radical strategy to solving the Auger decay problem is through the development of approaches that could allow realization of optical gain in the single-exciton regime, for which Auger recombination is simply inactive.[30] One such approach, which involved the use of type-II core/shell hetero-NCs, was recently demonstrated in ref 31. Spatial separation of electrons and holes in these nanostructures produces a significant imbalance between negative and positive charges,

* To whom correspondence shoule be addressed. E-mail: klimov@lanl.gov.

10.1021/jp0738659 CCC: $37.00
Published on Web 10/03/2007

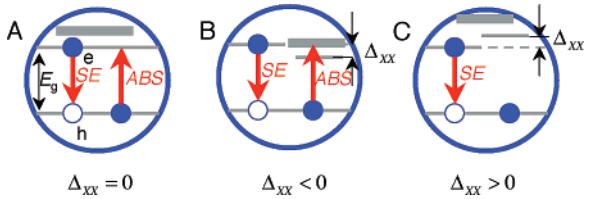

Figure 1. (A) In the absence of X−X interactions, excitation of a single electron−hole pair (single exciton) per NC on average does not produce optical gain but results in optical transparency, i.e., the regime for which stimulated emission is exactly compensated by absorption. The thin gray lines show states involved in the lowest energy emitting transition, while the thick gray line is the state involved in the higher-energy strong absorbing transition. (B,C) The balance between emission and absorption is broken if one accounts for X−X interactions, which spectrally displace the absorbing transition with respect to the emission band by Δ_{XX}. In the case of X−X attraction ($\Delta_{XX} < 0$), the transitions move downward in energy (shown in B), which may increase absorption at the emission wavelength because of the manifold of strong transitions located immediately above the emitting band. On the other hand, if the sign of Δ_{XX} is negative (X−X repulsion), absorbing transitions are moved upward in energy (shown in C), which leads to reduced absorption at the emission wavelength. If the transition shift induced by X−X repulsion is greater than the transition line width, optical gain can occur in the single-exciton regime.

which results in a strong local electric field. This field displaces the absorbing transition in singly excited NCs with respect to the emission line via the carrier-induced Stark effect and allows optical amplification due to single excitons.

Here, we develop a simple model for treating optical gain in NCs in the presence of X−X interactions for the arbitrary degeneracy (γ) of the emitting quantized states. This model shows that in the case when the X−X interaction is repulsive and its energy (Δ_{xx}) is greater than the ensemble line width (Γ) of the emitting transition, the optical-gain threshold reduces to $\langle N\rangle_{th} = \gamma/(\gamma + 1) < 1$. The latter expression indicates that lasing does *not* require multiexcitons and, hence, can be realized without complications associated with Auger recombination. Specifically, in the case of the 2-fold degeneracy of the emitting states, the gain threshold requires that only two-thirds of the NCs in the ensemble contain single excitons, while the rest remains unexcited. Further, we demonstrate both theoretically and experimentally that giant X−X repulsions with energies more than 100 meV can be obtained using type-II hetero-NCs of compositions such as CdS (core)/ZnSe (shell) and ZnTe (core)/CdSe (shell). Finally, we perform side-by-side comparison of transient-absorption spectra and dynamics for type-II CdS/ZnSe NCs and traditional type-I CdSe NCs. We observe a significant difference in optical-gain properties for these two types of the nanostructures, which points toward the single-exciton nature of light amplification in type-II NCs.

Single-Exciton Gain Model. The concept of single-exciton lasing using X−X repulsion was first introduced by us in 2004 in ref 30. It is clarified in Figure 1, in which we consider competition between absorption and stimulated emission (SE) in NCs (A) without and (B,C) with taking into account X−X Coulomb interactions. In the absence of X−X coupling, excitation of a single e−h pair (single exciton) per NC on average does not produce optical gain but results in optical transparency, that is the regime for which SE is exactly compensated by absorption (Figure 1A). The balance between SE and absorption is broken if one accounts for X−X interactions, which spectrally displaces the absorbing transition by Δ_{xx} with respect to the emission band in the presence of a single excited e−h pair.[32,33]

The effect of Coulomb interactions on optical gain depends upon the sign of the interaction energy because it determines the direction of the shift of the absorbing transitions with respect to the emission line. If Δ_{XX} is negative (X−X attraction), the transitions move downward in energy (Figure 1B), which may have a detrimental effect on lasing performance because of increasing absorption due to the manifold of strong transitions located immediately above the emitting band. On the other hand, the negative sign of Δ_{XX} (X−X repulsion) should benefit lasing because it shifts strongly absorbing transitions away from the emission line (Figure 1C). If the transition shift induced by X−X repulsion (i.e., X−X interaction energy) is greater than the ensemble line width, optical gain can occur in the single-exciton regime.

In monocomponent NCs or type-I NC heterostructures (both are referred below as type-I NCs), carrier−carrier Coulomb interactions tend to spatially arrange charges in such a way that the biexciton energy (E_{XX}) is reduced compared to twice the single-exciton energy (E_X).[34] This situation corresponds to the negative value of Δ_{XX} ($\Delta_{XX} = E_{XX} - 2E_X$), which can be interpreted in terms of effective X−X attraction. The X−X interaction strength is also often characterized by the biexciton binding energy (δE_{XX}), which relates to Δ_{xx} by $\delta E_{XX} = -\Delta_{XX}$. On the basis of this definition, X−X attraction corresponds to positive biexciton binding energies.

It is possible to reverse the sign of the X−X interaction energy using type-II heterostructures, in which the lowest energy states for electrons and holes reside in different regions of the hetero-NC.[35] In this case, the spatial distribution of charges is controlled not by Coulomb interactions but by large energy gradients at the core/shell interface that lead to concentration of the same-sign charges in the same part of the hetero-NC (both electrons are in the core and both holes are in the shell or vice versa) while it spatially separates charges of the opposite sign across the heterointerface (Figure 2A). This type of spatial arrangement increases the repulsive component of the Coulomb interaction and decreases its attractive component, which produces a net X−X repulsion (negative biexciton binding energy). A theoretical treatment of Coulomb interactions in hetero-NCs indicates that using a core/shell geometry one can obtain giant interaction energies of ~100 meV.[35]

To model optical gain in the presence of X−X repulsion, we assume that both electron and hole states involved in the emitting transition have the same degeneracy γ. The latter assumption describes well NCs of IV−VI lead salt compounds, which are characterized by nearly identical conduction- and valence-band electronic structures that result in the identical 8-fold degeneracy of electron and hole states.[23] The validity of this assumption is less obvious in the case of II−VI or III−V compounds. In these materials, the degeneracy of the lowest energy electron band is 2, while γ is greater than 2 for holes because of the complex, multi-subband character of the valence band. However, the state degeneracy can change in quantum-confined NCs. Specifically, the degeneracy of the lowest energy hole state can decrease to 2 because of state splitting induced by shape anisotropy, crystal field effects, and electron−hole exchange interactions.

We consider an NC ensemble, which contains only either NCs excited with a single e−h pair or unexcited NCs. Their respective fractions are n_X and $n_0 = 1 - n_X$, and hence $\langle N\rangle = n_X$. In unexcited NCs, both valence-band states are occupied with electrons and, therefore, these NCs can only absorb

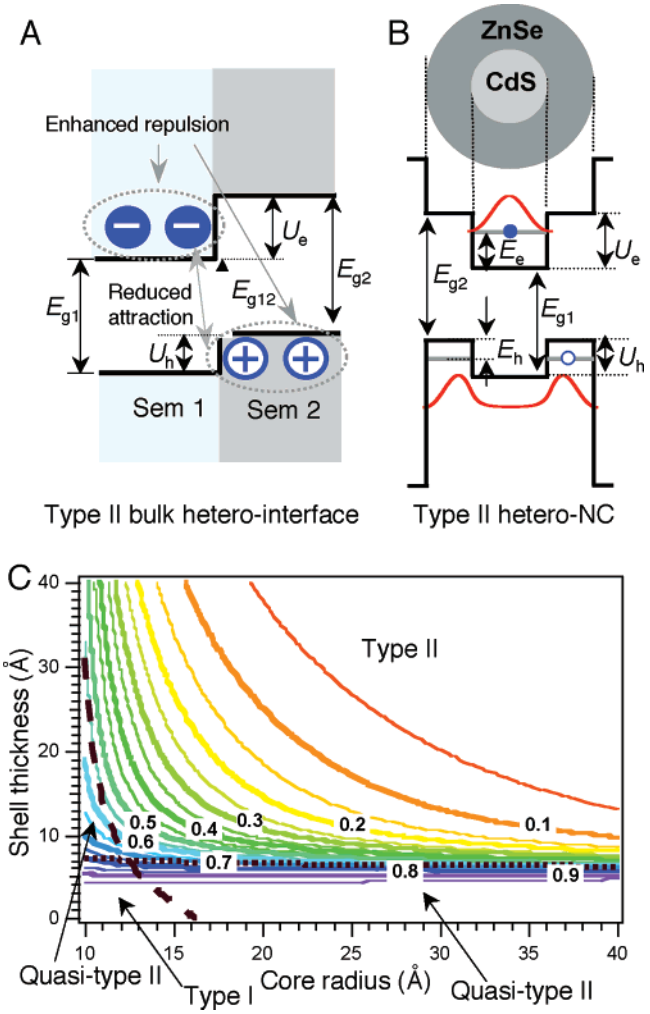

Figure 2. (A) In type-II heterostructures, the lowest energy states for electrons and holes are in different semiconductors. In this case, the spatial distribution of charges is controlled by energy gradients at the heterointerface, which leads to concentration of the same-sign charges in the same part of the heterostructure, while it spatially separates charges of the opposite sign across the heterointerface. This type of spatial arrangement of charges increases the repulsive component of the Coulomb interaction and decreases its attractive component, which produces net X−X repulsion (negative biexciton binding energy). (B) Energy diagram for a type-II CdS/ZnSe NC: $E_{g1} = 2.45$ eV, $E_{g2} = 2.72$ eV, $U_e = 0.8$ eV, and $U_h = 0.52$ eV ($T = 300$ K). (C) Contour plots of the e−h overlap integral calculated for CdS/ZnSe core/shell NCs as a function of CdS core radius, R, and ZnSe shell thickness, H. Black lines indicate the boundaries between type-I, quasi-type-II, and true-type II regimes. These boundaries are calculated using the "energy criterion" described in the text.

photons. The corresponding absorption cross section for photon energy $\hbar\omega$ is

$$\sigma_{11}^{0}(\omega) = A\frac{\gamma\Gamma_{11}^{2}}{(\hbar\omega - \hbar\omega_{11})^2 + \Gamma_{11}^{2}} \quad (1)$$

where $\hbar\omega_{11}$ and Γ_{11} are the energy and the homogeneous line width of the lowest-energy transition, respectively, $A = 4\pi\omega\langle|d_{11}|^2\rangle(n_r c\Gamma_{11})^{-1}$, in which $\langle|d_{11}|^2\rangle$ is the square of the transition dipole matrix element averaged over NC orientations, n_r is the refractive index, $\hbar$ is reduced Planck's constant, and c is the speed of light. The NCs excited with a single exciton produce both absorption and SE with cross sections σ_{11}^{X} and σ_{11}^{SE}, respectively. In the presence of X−X interactions, the absorption maximum is blue-shifted with respect to the SE maximum by the X−X interaction energy Δ_{XX} (Figure 1C).[32] Therefore, we can present $\sigma_{11}^{X}(\omega)$ and $\sigma_{11}^{SE}(\omega)$ as follows

$$\sigma_{11}^{X}(\omega) = A\frac{(\gamma - 1)\Gamma_{11}^{2}}{(\hbar\omega - \hbar\omega_{11} - \Delta_{XX})^2 + \Gamma_{11}^{2}}$$

and

$$\sigma_{11}^{SE}(\omega) = -A\frac{\Gamma_{11}^{2}}{(\hbar\omega - \hbar\omega_{11})^2 + \Gamma_{11}^{2}} \quad (2)$$

To calculate the absorption coefficient of an excited NC ensemble with the NC concentration n_{NC}, we account for the distribution of transition energies arising from NC size polydispersity, which leads to the following expression for a partial absorption coefficient due to the lowest energy transition.

$$\alpha_{11}(\omega) = n_{NC}\int_0^\infty [(1 - n_x)\sigma_{11}^{0} + n_x(\sigma_{11}^{X} + \sigma_{11}^{SE})]g(\omega_{11})\,d\omega_{11} \quad (3)$$

The distribution function $g(\hbar\omega_{11})$ in this expression is typically described by a Gaussian profile $g(\omega_{11}) = (\sqrt{\pi}\Gamma)^{-1}\exp(-(\hbar\omega_{11} - \hbar\omega_0)^2/\Gamma^2)$, where ω_0 is the central frequency of the lowest energy transition in the NC ensemble and Γ is its inhomogeneous line width. Assuming that the transition line widths of NC samples are dominated by inhomogeneous broadening, we can approximate the homogeneous line shape by the δ function: $\Gamma_{11}\pi^{-1}(x^2 + \Gamma_{11}^2)^{-1} \approx \delta(x)$. Using the latter expression in eq 3, we obtain

$$\alpha_{11}(\omega) = n_{NC}\frac{A\sqrt{\pi}\Gamma_{11}}{\Gamma}\exp\left(-\frac{\Delta^2}{\Gamma^2}\right)\left[\gamma - (\gamma + 1)n_X + (\gamma - 1)n_X\exp\left(-\frac{\Delta_{XX}^{2}}{\Gamma^2}\right)\exp\left(\frac{2\Delta\Delta_{XX}}{\Gamma^2}\right)\right] \quad (4)$$

where $\Delta = \hbar\omega - \hbar\omega_0$. Optical gain corresponds to the situation for which $\alpha_{11}(\hbar\omega) < 0$ and, hence, the gain threshold at $\omega = \omega_0$ can be calculated as $\langle N\rangle_{th} = n_X = \gamma(\gamma + 1 - (\gamma - 1)\exp(-\Delta_{XX}^2/\Gamma^2))^{-1}$. If $\Delta_{XX} \ll \Gamma$, it reduces to $\langle N\rangle_{th} = \gamma/2 \geq 1$, which corresponds to the usual multiexciton optical gain. However, if $\Delta_{XX} \gg \Gamma$, $\langle N\rangle_{th} = \gamma/(\gamma + 1) < 1$, which implies that in this case optical gain can be produced by single-exciton states without involvement of multiexcitons.

Using eq 4, we can calculate the maximum value of the optical gain (G_{max}), which can be achieved for the single-exciton mechanism. In the case of strong X−X interactions, SE from multiexcitons does not contribute to optical gain at the position of the single-exciton band. Therefore, maximum gain corresponds for the situation when all of the NCs are excited with single e−h pairs ($n_x = 1$). In this case,

$$G_{max}(\omega_0) = -\alpha_{11}(\omega_0) = n_{NC}\frac{A\sqrt{\pi}\Gamma_{11}}{\Gamma}\left[1 - (\gamma - 1)\exp\left(-\frac{\Delta_{XX}^{2}}{\Gamma^2}\right)\right] = \frac{1}{\gamma}\alpha_{11}^{0}(\omega_0)\left[1 - (\gamma - 1)\exp\left(-\frac{\Delta_{XX}^{2}}{\Gamma^2}\right)\right] \quad (5)$$

where $\alpha_{11}^{0}(\omega_0) = n_{NC}A\gamma\sqrt{\pi}\Gamma_{11}\Gamma^{-1}$ is the ensemble ground-state partial absorption coefficient, which corresponds to the

band-edge optical transition. In the case of strong X−X interactions ($\Delta_{XX} \gg \Gamma$), the maximum gain, which can be produced in the single-exciton regime in NCs with 2-fold degenerate emitting states, is one-half of the ground-state absorption coefficient.

The Effect of e−h Spatial Separation on the X−X Interaction Energy. Previously, we experimentally studied the effect of X−X interactions on optical-gain properties of NCs using ZnSe (core)/CdSe (shell) heterostructures.[29,30] The bulk ZnSe/CdSe heterointerface is characterized by the type-I alignment of energy states. However, in the case of hetero-NCs made up of these materials, there is a range of shell thickness for which an electron is localized in the shell while a hole is delocalized over the entire heterostructure volume. This situation corresponds to a partial spatial separation between electrons and holes (quasi-type-II regime[35]), which produces a reduced e−h overlap integral ($\Theta = |\langle\psi_h|\psi_e\rangle|^2$, where ψ_e and ψ_h are electron and hole wavefunctions) as indicated by radiative lifetime measurements.[36] Even this incomplete spatial separation between negative and positive charges results in improved optical-gain performance and, specifically, allows one to realize amplified spontaneous emission (ASE) in the range of green and blue colors that are difficult to obtain using traditional type-I CdSe-based NCs.[30] However, ASE in this case is still due to multiexcitons, and observed improvements in the optical-gain properties are primarily because of reduced Auger recombination rates and increased absorption cross sections.[29] The effect of energy shifts induced by X−X interactions is not apparent in these structures, likely because of the relatively small spatial separation between positive and negative charges that they produce.

Our recent modeling of Coulomb interactions in hetero-NCs indicates direct correlations between changes in the e−h overall integral and the strength of X−X coupling.[35] Specifically, this modeling shows that the X−X interaction energy rapidly increases as Θ decreases. Further, our calculations indicate that by using core/shell structures made of materials that are characterized by a type-II bulk heterointerface, one can obtain nearly complete spatial separation between electrons and holes, which results in giant X−X interaction energies on the order of 100 meV.

One type of nanostructure which we study here is CdS (core)/ZnSe (shell) NCs synthesized as described in ref 37. In the case of a bulk CdS/ZnSe heterojunction, the lowest energy states for electrons and holes are in different semiconductors (Figure 2A); therefore, the energy gradient at the interface tends to spatially separate electrons and holes across the boundary between different materials, which corresponds to the type-II behavior. The corresponding "spatially indirect" energy gap (E_{g12}) is determined by the energy separation between the conduction-band edge of one semiconductor and the valence-band edge of the other semiconductor. For the case shown in Figure 2A, E_{g12} can be related to conduction (U_c)- and valence (U_v)- band energy offsets at the interface by $E_{g12} = E_{g1} - U_h = E_{g2} - U_e$, where E_{g1} and E_{g2} are band gaps of semiconductors 1 and 2, respectively. In the case of a bulk CdS/ZnSe heterojunction, the room temperature indirect energy gap is ~1.93 eV, which is smaller than the energy gap of either of the material comprising the structure.

In contrast to the bulk situation with a "fixed" alignment of energy states at a heterointerface, the regime of carrier localization in core/shell CdS/ZnSe NCs depends on core radius (R) and shell thickness (H). Specifically, for a given R, it can change from type-I (both an electron and a hole are delocalized over the entire volume of the hetero-NC) to quasi type-II (hole is still delocalized over the entire hetero-NC volume while the electron resides primarily in the core) and finally to the true type-II regime (electron is in the core while hole is in the shell).[31,38] The latter situation is shown in Figure 2B.

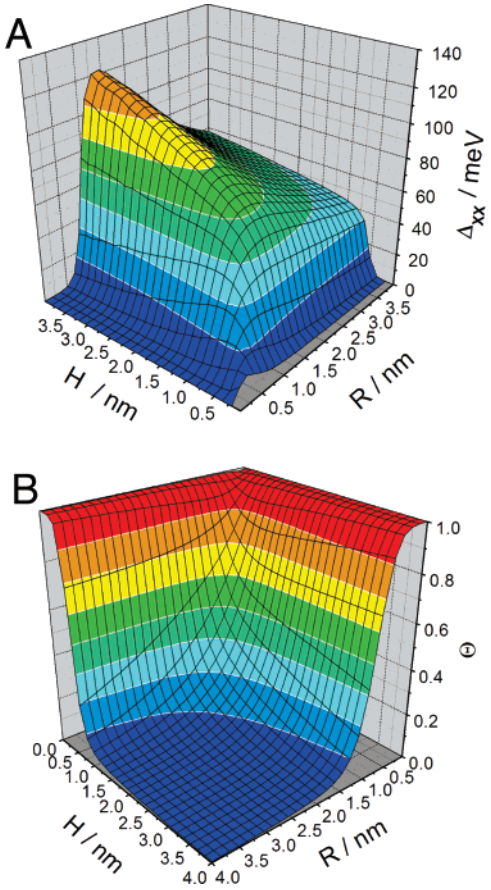

Figure 3. The X−X interaction energy, Δ_{XX} (A), and the e−h overlap integral, Θ (B), for CdS/ZnSe NCs as a function of core radius and shell thickness. These plots indicate that the increase in the degree of spatial separation between electrons and holes (i.e., decrease in Θ) correlates with the increase in the X−X repulsion energy.

Using the model described in ref 35, we calculate the e−h overlap integral as a function of R and H for CdS (core)/ZnSe (shell) NCs (Figure 2C). In the same plots, we also show boundaries between different localization regimes (type-I, quasi type-II, and type-II) calculated using the "energy criterion".[35] According to this criterion, an electron is primarily localized in the core if its lowest energy (1S) level is located below the conduction-band energy offset (U_e) at the core/shell interface (i.e., electron confinement energy E_e is smaller than U_e). On the other hand, a hole is shell localized if its confinement energy (E_h) is smaller than the valence-band energy offset (U_h).

Following the formalism developed in ref 35, we also analyze correlations between Θ and the X−X interaction energy for CdS/ZnSe hetero-NCs (Figure 3). We observe that for a fixed core radius, the increase in H leads to the increase in Δ_{XX} (at least initially). Further, for radii around 1.5 nm, the X−X interaction strength can reach giant values of more than 100 meV (Figure 3A). The Δ_{XX} growth correlates with the drop in Θ (Figure 3B) indicating that X−X interactions become enhanced with increasing degree of spatial separation between electrons and holes.

The effect of X−X repulsion is well manifested in type-II CdS (core)/ZnSe (shell) NCs.[39] Figure 4 shows a false-color

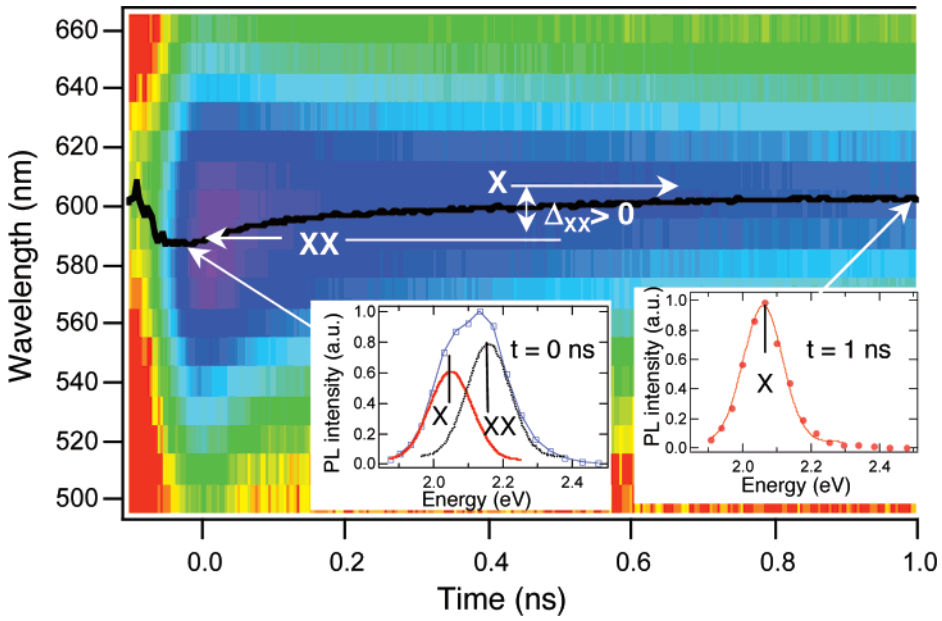

Figure 4. (A) A false-color plot of time and spectrally resolved emission intensity of CdS/ZnSe NCs ($R \approx 1.6$ nm, $H \approx 2$ nm) at $T = 300$ K recorded using excitation by 3 eV, 200 fs pulses (the color change from red to blue corresponds to the increase in the PL intensity, and the black line marks the position of the PL spectral maximum). Insets: instantaneous emission spectra (symbols) at $t = 0$ (left) and 1 ns (right). The $t = 0$ spectrum is deconvoluted into the single-exciton (X) and the biexciton (XX) bands (lines in the left inset).

plot of room-temperature, time-resolved photoluminescence (PL) of these NCs ($R \approx 1.6$ nm, $H \approx 2$ nm) taken using a time-correlated photon counting system (time resolution ~30 ps). The sample was excited with 200 fs pulses at 3 eV using a pump fluence, which corresponded to approximately 1.5 excitons per NC on average. According to the phase diagram in Figure 2C, these NCs are in the type-II region and, hence, they are expected to produce significant X−X repulsion. Indeed, this effect is apparent in spectrally resolved dynamics in Figure 4. On the basis of the excitation fluence used in these measurements, we estimate that nearly half (or more) of the photons emitted at early times after photoexcitation are due to biexcitons and, therefore, the initial part of the PL spectrum is significantly weighted toward the biexciton emission maximum. Following fast decay of biexcitons via Auger recombination, the PL maximum eventually approaches the position of the single-exciton band (ca. 300 ps after excitation for the sample in Figure 4). Therefore, the direction and the magnitude of the shift of the PL maximum in time-resolved spectra provide direct information on the sign and the strength of the X−X interactions.

In type-I NCs, in which the X−X interaction is attractive, the biexciton band is red-shifted with regard to the single-exciton emission.[34] The data in Figure 4 show the opposite shift, namely the biexcitonic emission observed at short time after excitation is blue-shifted with regard to single-exciton emission measured at later times. This result is indicative of X−X repulsion. To quantify the energy of X−X interaction, we compare two instantaneous PL spectra obtained by "slicing" the data in Figure 4 at times $t = 0$ and 1 ns. The long-time spectrum (red solid circles in the right inset of Figure 4) is identical to the steady-state PL spectrum measured at low excitation fluences ($\langle N \rangle << 1$), which confirms that it is primarily due to emission of single excitons ($E_X = 2.054$ eV). The $t = 0$ PL (blue open squares in the left inset of Figure 4) indicates the presence of an additional high-energy, short-lived band at 2.160 eV, which is due to emission from biexcitons. This band (XX feature) can be extracted from the $t = 0$ spectrum by subtracting an appropriately scaled longer time spectrum (X feature). From the spectral separation between the X and XX bands, we can determine the strength of X−X repulsion, which is 106 meV for the sample in Figure 4. This value is in good agreement with our calculations that predict the interaction energy of ~90 meV for NCs studied here. Further, the energy of X−X repulsion is greater than the width of the single-exciton emission line ($\Gamma \approx 80$ meV, as derived from a Gaussian fit) indicating the feasibility of significant suppression of absorption in singly excited NCs at the emission wavelength through X−X interactions.

We also observe a similar effect of strong X−X repulsion in type-II hetero-NCs of a different composition [ZnTe (core)/CdSe (shell)] with emission in the near-infrared (770 nm) region. This combination of materials provides the type-II energy offsets in the bulk form (Figure 5A). Therefore, appropriately engineered NCs also show a regime of true type-II localization, for which electrons reside in the shell and holes are in the core. This type of spatial separation is opposite to that observed in CdS (core)/ZnSe (shell) nanostructures, where electrons are core localized while holes are localized in the shell. In Figure 5B, we show a comparison of short- ($t = 0$) and long-time ($t = 5$ ns) PL spectra of ZnTe/CdSe NCs taken for $\langle N \rangle$ of ~2.5. The $t = 0$ spectrum can be deconvoluted into a single-exciton band at 1.586 eV and a blue-shifted biexciton band at 1.667 eV. From the positions of these bands, we can infer the X−X repulsion energy of ~80 meV. Recently, a similar effect of X−X repulsion (Δ_{XX} up to 30 meV) was also reported for type-II CdTe/CdSe NCs.[40] All of these results point toward the generality of large positive X−X interaction energies in strongly confined type-II colloidal nanoparticles.

Comparison of Optical-Gain Properties of Type-II and Type-I NCs. To study the effect of X−X interactions on optical gain, we perform comparative studies of optical-gain performance of type-II CdS/ZnSe NCs with that of traditional type-I CdSe NCs with similar emission wavelengths. To measure optical gain, we use an ultrafast transient absorption (TA) experiment, in which the absorption change ($\Delta\alpha$) induced in the sample by a 100 fs pump pulse at 3 eV is probed with a variably delayed, broad-band pulse of a femtosecond white-

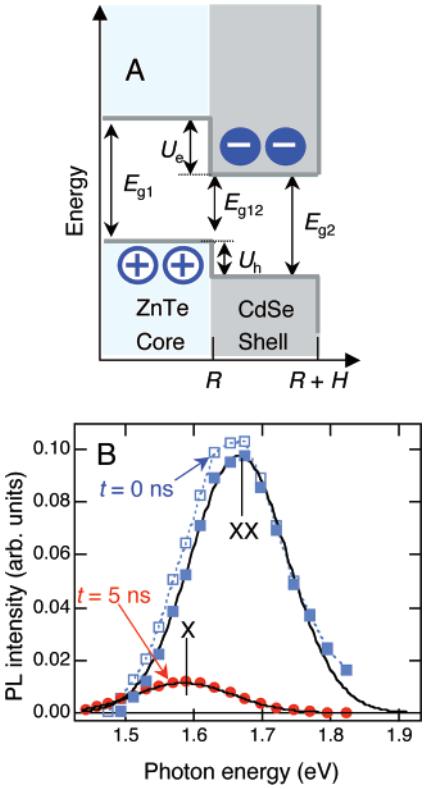

Figure 5. (A) Electronic structure of the type-II ZnTe/CdSe interface (E_{g1} = 2.26 eV, E_{g2} = 1.74 eV, U_e = 1.22 eV, U_h = 0.7 eV, and E_{g12} = 1.04 eV; T = 300 K). (B) Comparison of short- (t = 0 ns) and long-time (t = 5 ns) PL spectra of ZnTe (core)/CdSe (shell) NCs (300 K), which indicates the X−X repulsion with the energy of ~80 meV.

light continuum.[41] Optical gain corresponds to the situation for which the absorption bleaching ($\Delta\alpha < 0$) is greater than the absorption coefficient of the unexcited samples (α_0): $-\Delta\alpha/\alpha_0 > 1$. In this case, the absorption coefficient of the excited sample ($\alpha = \alpha_0 + \Delta\alpha$) is negative: $\Delta\alpha < 0$.

Figure 6 shows PL and pump-intensity-dependent absorption spectra of traditional core-only CdSe NCs (A) and type-II CdS/ZnSe NCs (B). The type-II core−shell sample is prepared as a hexane solution, while CdSe is dissolved in trioctylphosphine (TOP), which is one of the solvents used for growing CdSe NCs. The use of TOP instead of hexane allows us to reduce interference from photoinduced absorption, which competes with optical gain in NC solution samples and is presumably due to NC interface states.[42] The effect of the photoinduced absorption at the position of the gain band was not significant in type-II samples.

Both CdSe and CdSe/ZnSe samples show the development of optical gain (negative α) at high pump fluences. Optical-gain properties of these two types of samples, however, are distinctly different. In type-I CdSe NCs, the gain band is red-shifted with regard to the center of the PL band (Figure 6A) and its initial growth is nearly quadratic in pump fluence (Figure 6C, open and solid blue squares). Both of these observations are consistent with the fact that optical gain occurs primarily due to doubly excited NCs (biexcitons). The number of these NCs scales as the pump fluence squared, and their emission is red-shifted with respect to the single-exciton band because of X−X attraction in type-I structures.[21,34] We observe that the gain threshold is higher than a theoretical value of $\langle N\rangle = 1$ expected for the biexcitonic mechanism, which is likely because of the competing contribution from photoinduced absorption[42] and losses due to light scattering.

In the type-II sample, the gain first develops near the center of the PL band and then extends to higher spectral energies at higher pump fluences (Figure 6B). The development of gain occurs approximately linearly with the pump fluence (Figure 6D, open and solid red circles). The gain threshold is reduced compared to that in type-I NCs and is ca. 0.8, which is close to the theoretical value of 0.66 expected for the single-exciton regime in the case of the 2-fold degenerate emitting states. All of these observations are consistent with the fact that optical amplification observed in these experiments is due to single excitons. Further, the $\Delta\alpha$ growth at the center of the PL band can be closely described by the dependence $1.5\langle N\rangle$ as predicated by eq 4 for the single-exciton gain mechanism for the case of $\gamma = 2$. The broadening of the gain band toward higher energies observed at high pump levels is likely to due the contribution from "repulsive" biexcitons.

A distinct difference between optical-gain regimes in type-I and type-II structures is also evident from the $\Delta\alpha$ dynamics measured at the onset of optical gain for CdSe NCs (inset of Figure 6C) and CdS/ZnSe NCs (inset of Figure 6D). These data indicate that the relaxation time constant is longer by more than a factor of 50 in type-II NCs compared to that in type-I NCs (1700 vs 30 ps). The fast decay in CdSe NCs is due to Auger recombination of multiexcitons that provide a significant contribution to TA signals at the onset of the optical-gain regime. On the other hand, the contribution from multiexcitons to $\Delta\alpha$ at the gain threshold in CdS/ZnSe NCs is not large, and therefore, the observed relaxation is primarily due to decay of singly excited NCs. The PL quantum yield of core/shell samples studied here did not exceed 25%, and therefore, the exciton relaxation was dominated not by radiative decay but more likely by surface trapping (see ref 37 for the analysis of the effect of various NC surface- and core/shell-interface-treatment procedures on PL efficiencies of hetero-NCs). The improvement in the sample quality should allow for the increase of the single-exciton lifetime potentially to the radiative recombination limit, which is ~100 ns for samples used in this work.

To further confirm that $\Delta\alpha$ at the position of the PL X feature does not have an appreciable contribution from multiexcitons, we compare the dynamics shown in the inset of Figure 6D with those of Auger decay of the biexcitons. To measure the biexciton Auger lifetime (τ_2) of core/shell samples, we monitor pump-intensity-dependent TA dynamics near the position of the XX PL feature (Figure 6E). The corresponding excitation densities ($\langle N\rangle$ from 0.06 to 0.6) are in the range where photoexcited NCs are primarily either in a single-exciton or in a biexciton state. The recorded time transients can be fit to a double-exponential decay ($A_f \exp(-t/\tau_f) + A_s \exp(-t/\tau_s)$, where $A_f(\tau_f)$ and $A_s(\tau_s)$ are the amplitudes (time constants) of the fast and the slow decay components, respectively) using a single fast time constant of 210 ps and a slow decay constant of ~4−20 ns, which we attribute to relaxation of biexcitons and single excitons, respectively. This assignment is consistent with the pump intensity dependence of amplitudes A_f and A_s (Figure 6F). The A_s amplitude shows sublinear growth that can be described by the Poissonian probability, p_1, for absorbing a single photon per NC; $p_1 = \langle N\rangle \exp(-\langle N\rangle)$ (we neglect a small contribution from "secondary" excitons generated via decay of biexcitons). On the other hand, the A_f amplitude shows superlinear growth, which is consistent with the $\langle N\rangle$-dependent variation of the Poissonian probability, p_2, for absorbing two photons per NC; $p_2 = 0.5(\langle N\rangle)^2 \exp(-\langle N\rangle)$. The biexciton life time derived from these measurements (210 ps) is significantly shorter than the decay time constant in the inset of Figure 6D, which indicates

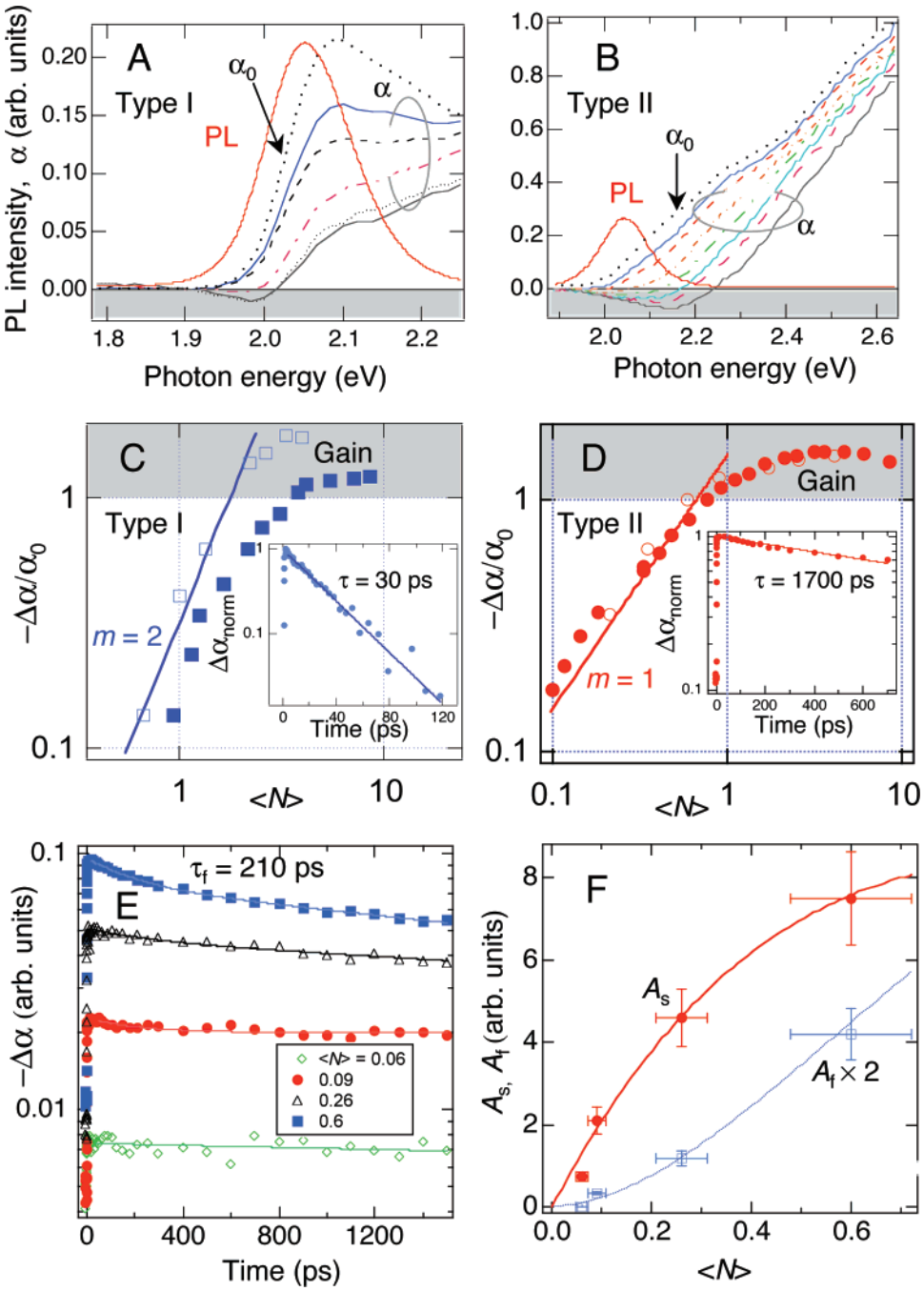

Figure 6. (A,B) Absorption spectra of unexcited (α_0) and excited (α) samples of type-I CdSe NCs with $R = 2.3$ nm (in A) and type-II CdS/ZnSe NCs (in B, the same sample as in Figure 4) in comparison to their emission bands. The spectra of α are taken using pump fluences that increase from the upper to the lower spectrum (0.1−2 mJ cm^{-2} (A) and 0.2−5 mJ cm^{-2} (B)). In both cases, we observe the development of optical gain, which corresponds to $\alpha < 0$ (the area shown in gray). (C,D) The dependence of normalized absorption bleaching in type-I (open and solid blue squares in C) and type-II (open and solid red circles in D) NCs as a function of $\langle N \rangle$ in comparison to linear (red straight line) and quadratic (blue straight line) growth. The area shown in gray corresponds to optical gain ($-\Delta\alpha/\alpha_0 > 1$). Red open circles are the data derived from spectra of the type-II sample in panel B, while red solid circles are independent measurements for a different type-II sample with a similar emission wavelength. Blue open squares are from pump-fluence-dependent spectra of CdSe NCs in a TOP solution, while blue solid squares are the independent measurements for a solid-state film of CdSe NCs. Insets: TA dynamics at the optical-gain onset measured for the type-I (C) and type-II (D) samples. (E) TA dynamics (symbols) measured at 2.12 eV for different pump fluences (corresponding values of $\langle N \rangle$ are indicated in the figure); lines are double-exponential fits. (F) The pump dependence of the amplitudes of the fast (A_f) and slow (A_s) decay components (symbols) derived from fits to data in panel E in comparison to Poissonian probabilities p_1 and p_2 (see text for details).

that $\Delta\alpha$ at the position of the single-exciton emission band is not significantly contributed by biexcitons (at least near the optical-gain threshold).

The τ_2 constant of the core/shell samples studied is approximately twice as long as that of traditional type-I CdSe NCs emitting at a similar wavelength.[24] Analogous lengthening of Auger time constants was also observed for quasi-type-II ZnSe/CdSe NCs.[29] Theoretical understanding of the effect of e−h spatial separation on Auger recombination is still lacking. Recently, Oron et al. suggested that the rate of Auger decay in type-II NCs should be affected by the reduction in the e−h overlap integral, which could result in significant extension (up to nanoseconds) of Auger lifetimes.[40] Specifically, they proposed that the biexciton Auger decay time in type-II heterostructures

should scale as the product of the NC volume (V) and the radiative lifetime (τ_r; it is inversely proportional to the e−h overlap integral), which was a generalization of the $\tau_2 \propto V$ scaling previously established for the traditional type-I NCs.[24] While e−h overlap may indeed affect the rates of Auger decay, the overall effect of e−h spatial separation on Auger rates is likely more complex than is suggested by scaling from ref 40. Specifically, this scaling does not account for factors, such as a significant increase in the strength of X−X coupling upon spatial separation of positive and negative charges, which should affect the Auger decay rate. For example, as indicated by the results of our modeling in Figure 3, the reduction in the e−h overlap integral directly correlates with the increase in the X−X interaction energy; the resulting changes in the Auger recombination rate will dependent upon interplay between these two competing trends.

Using the TA results, we can estimate a maximum value of the optical-gain cross section of the hetero-NCs (σ_g). The pump-intensity-dependent data in Figure 6D indicate that $|\Delta\alpha|$ measured at the position of the single-exciton transition (∼2.05 eV) attains saturation at a value of approximately $1.5\alpha_0$, which corresponds to the optical-gain coefficient of $0.5\alpha_0$. The latter quantity is consistent with the maximum gain expected for the single-exciton regime (eq 5, $\gamma = 2$). We further estimate that the single-exciton gain cross section is ca. 1.3×10^{-17} cm^2. The gain cross section for the biexciton band (∼2.15 eV) is approximately twice as large ($\sim 2 \times 10^{-17}$ cm^2), which might be indicative that the radiative rate of a biexciton in these NCs is twice the rate as that of a single exciton.

Using the TA data in Figure 6A, we can also estimate σ_g for the biexcitonic gain in type-I CdSe NCs. These estimations yield $\sigma_g \approx 5 \times 10^{-17}$ cm^2, which is greater than σ_g for the type-II NCs. The latter result is expected based on the greater oscillator strength of the "spatially direct" optical transition in type-I structures compared to that of the "spatially indirect" transition in type-II structures.

Conclusions and Outlook

We have performed the analysis of optical gain in semiconductor NCs in the presence of strong X−X interactions. This analysis indicates that if the X−X interaction is repulsive and its energy is greater than the ensemble line width of the emitting transition, the gain threshold in the case of 2-fold-degenerate emitting states approaches the value of $^2/_3$ (defined in terms of average number of e−h pairs per NC). This result implies that in this case optical amplification does not require multiexcitons and can occur by SE from single excitons. To practically realize strong X−X repulsion, we develop type-II core/shell heterostructures of compositions CdS (core)/ZnSe (shell) and ZnTe (core)/CdSe (shell). These nanostructures show giant Coulomb repulsion energies of more than 100 meV, which is consistent with the results of our modeling of biexciton energies in ref 35. Using CdS/ZnSe hetero-NCs, we experimentally demonstrate optical amplification using single-exciton states, which provides experimental validation for the concept of single-exciton gain using exciton−exciton repulsion introduced by us in ref 30.

An important implication of this work is that it points toward a practical approach for overcoming a major complication for NC lasing arising from ultrafast Auger recombination of multiexcitons.[6,24] In traditional type-I NCs, in which the Coulomb X−X interaction is attractive and its energy is smaller than typical inhomogeneous transition line widths, optical gain occurs due to SE from multiexcitons. As a result, the intrinsic decay of optical gain is dominated by Auger recombination, which limits its lifetime to picosecond timescales.[43] By implementing single-exciton gain strategies, one can change the nature of the optical-gain relaxation process from Auger recombination of multiexcitons to radiative decay of single excitons. In type-I NCs of II−VI compounds, for example, radiative recombination is characterized by time scales of tens of nanoseconds.[44,45] Because of reduced e−h overlap, the time constants are expected to be even longer in type-II structures.[36,40,46] This should allow for significant extension of optical-gain lifetimes (potentially, by orders of magnitude). The latter should simplify realization of lasing under steady-state excitation using optical and perhaps electrical pumping.

The impact of this work can be can be particularly significant in the case of NCs with highly degenerate emitting states. In PbSe NCs, for example, the lowest energy electron and hole states are 8-fold degenerate, which leads to high optical-gain threshold of four excitons per NC on average.[22] This high exciton multiplicity further results in very short gain lifetimes because of rapid shortening of the Auger time constants with the number of excitons. Using single-exciton gain regime one can reduce the gain threshold to below unity and simultaneously greatly increase optical-gain lifetimes.

Acknowledgment. This work was supported by the Chemical Sciences, Biosciences, and Geosciences Division of the Office of Basic Energy Sciences, U.S. Department of Energy (DOE), Los Alamos LDRD funds, and the Center for Integrated Nanotechnologies jointly operated by Los Alamos and Sandia National Laboratories for the DOE.

References and Notes

(1) Bruchez, M.; Moronne, M.; Gin, P.; Weiss, S.; Alivisatos, A. P. *Science* **1998**, *281*, 2013.
(2) Dubertret, B.; Skourides, P.; Norris, D. J.; Noireaux, V.; Brivanlou, A. H.; Libchaber, A. *Science* **2002**, *298*, 1759
(3) Colvin, V. L.; Schlamp, M. C.; Alivisatos, A. P. *Nature* **1994**, *370*, 354.
(4) Dabbousi, B. O.; Bawendi, M. G.; Onitsuka, O.; Rubner, M. F. *Appl. Phys. Lett.* **1995**, *66*, 1316.
(5) Achermann, M.; Petruska, M. A.; Kos, S.; Smith, D. L.; Koleske, D. D.; Klimov, V. I. *Nature* **2004**, *429*, 642.
(6) Klimov, V. I.; Mikhailovsky, A. A.; Xu, S.; Malko, A.; Hollingsworth, J. A.; Leatherdale, C. A.; Eisler, H. J.; Bawendi, M. G. *Science* **2000**, *290*, 314.
(7) Eisler, H.-J.; Sundar, V. C.; Bawendi, M. G.; Walsh, M.; Smith, H. I.; Klimov, V. I. *Appl. Phys. Lett.* **2002**, *80*, 4614.
(8) Efros, A. L.; Efros, A. L. *Sov. Phys. Sem.* **1982**, *16*, 772.
(9) Brus, L. E. *J. Chem. Phys.* **1983**, *79*, 5566.
(10) Murray, C. B.; Kagan, C. B.; Bawendi, M. G. *Science* **1995**, *270*, 1335.
(11) Olsson, Y. K.; Chen, G.; Rapaport, R.; Fuchs, D. T.; Sundar, V. C.; Steckel, J. S.; Bawendi, M. G.; Aharoni, A.; Banin, U. *Appl. Phys. Lett.* **2004**, *85*, 4469
(12) Sundar, V. C.; Eisler, H.-J.; Bawendi, M. G. *Adv. Mater.* **2002**, *14*, 739.
(13) Petruska, M. A.; Malko, A. V.; Voyles, P. M.; Klimov, V. I. *Adv. Mater.* **2003**, *15*, 610.
(14) Klimov, V. I.; Bawendi, M. G. *MRS Bull.* **2001**, *26*, 998.
(15) Kazes, M.; Lewis, D. Y.; Evenstein, Y.; Mokari, T.; Banin, U. *Adv. Mater.* **2002**, *14*, 317.
(16) Malko, A. V.; Mikhailovsky, A. A.; Petruska, M. A.; Hollingsworth, J. A.; Htoon, H.; Bawendi, M. G.; Klimov, V. I. *Appl. Phys. Lett.* **2002**, *81*, 1303.
(17) Hines, M. A.; Guyot-Sionnest, P. *J. Phys. Chem.* **1996**, *100*, 468.
(18) Peng, X.; Schlamp, M. C.; Kadavanich, A. V.; Alivisatos, A. P. *J. Am. Chem. Soc.* **1997**, *119*, 7019.
(19) Dabbousi, B. C.; Rodriguez-Viejo, J.; Mikulec, F. V.; Heine, J. R.; Mattoussi, H.; Ober, R.; Jensen, K. F.; Bawendi, M. G. *J. Phys. Chem. B* **1997**, *101*, 9463.
(20) Qu, L.; Peng, X. *J. Am. Chem. Soc.* **2002**, *124*, 2049.
(21) Mikhailovsky, A. A.; Malko, A. V.; Hollingsworth, J. A.; Bawendi, M. G.; Klimov, V. I. *Appl. Phys. Lett.* **2002**, *80*, 2380.

(22) Schaller, R. D.; Petruska, M. A.; Klimov, V. I. *J. Phys. Chem. B* **2003**, *107*, 13765.

(23) Kang, I.; Wise, F. W. *J. Opt. Soc. Am. B* **1997**, *14*, 1632.

(24) Klimov, V. I.; Mikhailovsky, A. A.; McBranch, D. W.; Leatherdale, C. A.; Bawendi, M. G. *Science* **2000**, *287*, 1011.

(25) Chatterji, D. *The Theory of Auger Transitions*; Academic Press: London, 1976.

(26) Landsberg, P. T. *Recombination in Semiconductors*; University Press: Cambridge, 1991.

(27) Htoon, H.; Hollingsworth, J. A.; Dickerson, R.; Klimov, V. I. *Phys. Rev. Lett.* **2003**, *91*, 227401.

(28) Htoon, H.; Hollingsworth, J. A.; Malko, A. V.; Dickerson, R.; Klimov, V. I. *Appl. Phys. Lett.* **2003**, *82*, 4776.

(29) Nanda, J.; Ivanov, S. A.; Htoon, H.; Bezel, I.; Piryatinski, A.; Tretiak, S.; Klimov, V. I. *J. Appl. Phys.* **2006**, *99*, 034309.

(30) Ivanov, S. A.; Nanda, J.; Piryatinski, A.; Achermann, M.; Balet, L. P.; Bezel, I. V.; Anikeeva, P. O.; Tretiak, S.; Klimov, V. I. *J. Phys. Chem. B* **2004**, *108*, 10625.

(31) Klimov, V. I.; Ivanov, S. A.; Nanda, J.; Achermann, M.; Bezel, I.; McGuire, J. A.; Piryatinski, A. *Nature* **2007**, *447*, 441.

(32) Klimov, V.; Hunsche, S.; Kurz, H. *Phys. Rev. B* **1994**, *50*, 8110.

(33) Klimov, V. I. *J. Phys. Chem. B* **2000**, *104*, 6112.

(34) Achermann, M.; Hollingsworth, J. A.; Klimov, V. I. *Phys. Rev. B* **2003**, *68*, 245302.

(35) Piryatinski, A.; Ivanov, S. A.; Tretiak, S.; Klimov, V. I. *Nano Lett.* **2007**, *7*, 108.

(36) Balet, L. P.; Ivanov, S. A.; Piryatinski, A.; Achermann, M.; Klimov, V. I. *Nano Lett.* **2004**, *4*, 1485.

(37) Ivanov, S. A.; Piryatinski, A.; Nanda, J.; Tretiak, S.; Werder, D.; Klimov, V. I. *J. Am. Chem. Soc*. **2007**, DOI: 10.1021/ja068351m.

(38) Piryatinski, A.; Ivanov, S. A.; Tretiak, S.; Klimov, V. I. *Nano Lett.* **2007**, *7*, 108.

(39) Ivanov, S. A.; Bezel, I. V.; Nanda, J.; Piryatinski, A.; Achermann, M.; Klimov, V. I. Amplified spontaneous emission in the single-exciton regime using colloidal type II core/shell nanocrystals. Fourth International Conference on Semiconductor Quantum Dots, Chamonix-Mont Blanc, France, 2006.

(40) Oron, D.; Kazes, M.; Banin, U. *Phys. Rev. B* **2007**, *75*, 035330/1.

(41) Klimov, V. I.; McBranch, D. W. *Opt. Lett.* **1998**, *23*, 277.

(42) Malko, A. V.; Mikhailovsky, A. A.; Petruska, M. A.; Hollingsworth, J. A.; Klimov, V. I. *J. Phys. Chem. B* **2004**, *108*, 5250.

(43) Mikhailovsky, A. A.; Xu, S.; Klimov, V. I. *Rev. Sci. Instrum.* **2002**, *73*, 136.

(44) Crooker, S. A.; Barrick, T.; Hollingsworth, J. A.; Klimov, V. I. *Appl. Phys. Lett.* **2003**, *82*, 2793.

(45) Labeau, O.; P. Tamarat; Lounis, B. *Phys. Rev. Lett.* **2003**, *90*, 257404.

(46) Kim, S.; Fisher, B.; Eisler, H.-J.; Bawendi, M. G. *J. Am. Chem. Soc.* **2003**, *125*, 11466.